Int. J. Electrochem. Sci., 15 **(2020)** 5927 – 5944, doi: 10.20964/2020.03.10

International Journal of ELECTROCHEMICAL SCIENCE
www.electrochemsci.org

A Sensitive Electrochemical Sensor Based on Au@Pd Hybrid Nanorods Supported on B-doped Graphene for Simultaneous Determination of Acetaminophen, Dopamine and Tyrosine

Xianlan Chen[1,2], Guowei Zhang[1,2], Ying He[1,2], Ling Shi[1,2],Jucheng Zhang[1,2], Guangming Yang[1,2,], Haibo Pan[3], Wei Liu[*1,2], Shaoping Feng[1,2,*]*

[1] School of Science, Honghe University
[2] Key Laboratory of Natural Pharamaceutical & Chemical Biology of Yunnan Province Mengzi, Yunnan 661100, P.R.China
[3] Fujian Key Lab of Medical Instrument & Pharmaceutical Technology, Yishan Campus, Fuzhou University, Fuzhou, Fujian 350002, China
[*]E-mail: 13489086418@163.com; yangguangmingbs@126.com; liuwei4728@126.com; shaopingfeng@126.com

Received: 21 August 2019 / *Accepted:* 28 December 2019 / *Published:* 10 May 2020

In this report a fast and sensitive electrochemical sensor for simultaneous determination of DA, AC and Tyr was proposed based on the Au@Pd HNRs/BG hybrid nanocomposites. Firstly, the incorporation of B atom into graphene with porous framework was achieved by one-pot hydrothermal approach. Secondly, the Au@Pd hybrid nanorods (Au@Pd HNRs) were encapsulated in B-doped graphene (BG) to form Au@Pd HNRs/BG hybrid nanocatalysts. Interestingly, boron-doping effect introduce the highly dispersed COOH groups and abundant defect sites, which not only improve the interfacial properties of Au@Pd HNRs, resulting ultrathin BG effectively enwrapped most of individual Au@Pd HNRs with excellent dispersibility, but the -COOH units form hydrogen bonding with the phenolic hydroxyl groups of DA, AC and Tyr, which provide a large specific surface area to increase their loading amount and improve the excellent electro-catalytic effect the three analytes. Therefore, high enough anodic peaks potential separation of DA, AC and Tyr and increased peak currents at Au@Pd HNRs/BG/GCE was provided a simultaneous sensitively determination of them with extraordinary stability and cost effective analysis, the detection limits (S/N=3) for determination of DA, AC and Tyr were found to be 4.58, 6.35 and 3.71 μM, respectively. Finally, the as-fabricated sensor was satisfactorily used for the determination of DA, AC and Tyr in the urine sample with acceptable recovery range.

Keywords: Dopamine, Acetaminophen, Tyrosine, Au@Pd HNRs/BG hybrid nanocomposites, Simultaneous determination

1. INTRODUCTION

Dopamine (3, 4-dihydroxyphenylethylamine, DA) is belongs to a group of catecholamines, which plays a significant role in the functioning of the mammalian central nervous, cardiovascular, renal and hormonal systems as well as necessity to monitor HIV infection and diagnose Parkinson's disease [1]. DA can also be used widely as a medicine, however in high doses and drug addiction it can lead to increased heart rate and blood pressure [2]. Tyrosine (4-Hydroxyphenylalanine, Tyr) is a non-essential amino acid synthesized from phenylalanine, which can be a main target for radical's attack as antioxidant and indispensable for human to establish and maintain nutritional balance. Its absence could may lead to albinism, atherosclerosis, alkaptonuria, depression, hypochondria and other psychological diseases while a high level of Tyr could cause the increase of sister chromatid exchange [3]. In the human body, Tyr plays a major role in the synthesis of the neurotransmitter serotonin such as norepinephrine and DA. Moreover, Tyr is a precursor of the epinephrine and catecholamine neurotransmitters enhance mood and cognitive function especially under situations involving stress or when DA levels require additional support [4]. Acetaminophen (N-acetyl-p-aminophenol, AC) or paracetamol is a widely used analgesic and antipyretic drug, which is commonly used for the reduction of fever and as a pain killer for the relief of headaches pain, other minor aches and pains (backache, arthritis and postoperative pain), and is a major component in numerous cold and flu drugs [5]. AC is clinically important, though overdosing and chronic use in AC levels may lead to toxic metabolites accumulation in kidney and liver, causing fatal hepatoxicity and nephrotoxicity [6]. The overdose of AC in vivo models has been found to AC protects dopaminergic neurons from the oxidative stress damage caused by acute exposure to higher levels of DA [7]. Moreover, H. Karimi-Maleh have confirmed that nitrated tyrosine residues and AC adducts can be found in necrotic cells after being subjected to overdosage of AC [8]. On the other hand, DA, AC and Tyr have associated with each other, therefore, it is importance simultaneous determination of the mentioned analytes in biologic fluids and pharmaceutical is indispensable [7,9].

DA, Tyr and AC contain phenolic hydroxyl group, which is electrochemically active and can be oxidized. However, it is well-known that their oxidation potentials on the conventional electrodes usually overlapping voltammetric responses, even no peak appears at lower concentrations [10]. Fortunately, various electrochemical modified electrodes were fabricated and applied for effective analysis of a mixture of these biomolecules in recent years, because of their good sensitivity, simplicity, good stability and low cost are the better choice for simultaneously determination of these compounds [10]. For instances, Liu et al. fabricates a sensitive electrochemical sensor based on nickel and copper oxides-decorated graphene composite (NiO–CuO/GR/GCE) for simultaneous determination of DA, AC and tryptophan using square wave voltammetry [11]. F. Tadayon et al. have been reported the simultaneous voltammetric determination of AA, AC and Ty using Au-Pd/reduced graphene oxide composite as a new sensing layer [3]. M. Taei et al. constructed a novel Au-nanoparticles/poly-(2-amino-2-hydroxymethyl-propane-1, 3-diol) film modified glassy carbon electrode (AuNPs/poly(trisamine)/GCE) for the concurrent electrochemical detection of norepinephrine, AC and Tyr [12]. Thus it can be seen that a multitudinous of novel electrode materials, such as polymers, transition metaloxides, graphene and noble metal nanoparticle, were introduced and capable of electrocatalytic oxidation of DA, Tyr and AC.

For the above considerations, the performance of modified electrodes are mainly depended on the properties of electro-catalysts. The electrode nanomaterials act as conduction centers facilitating the transfer of electrons and provide great catalytic surface areas, improving the selectivity and separating the signals of co-existing molecules from each other. In our previous study, we have found that B-doping graphene (BG) not only can modify the electronic band structure of graphene, tuning the mechanical properties and electrocatalytic activity, but boron can acts as an electron acceptor improving adsorption properties and electron transport rate. In particular, B-doped graphene was prepared by hydrothermal approach with some dispersed carboxyl units were prepared by hydrothermal approach, which can form hydrogen bonding with the phenolic hydroxyl groups of DA, Tyr and AC, making more target biomolecules enrich easily on modified electrode surface and directly monitor them.

For electrochemical signal amplifying, another effective strategy often used is introducing noble metal nanomaterials as electron mediators in detection systems. Gold nanorods (Au NRs) with well-defined and controllable shapes and aspect ratios were used as ideal candidates for electrode materials in electrochemical sensors and provided multiple electron pathways because of their attractive advantages such as facile and rapid preparation technique, excellent electronic properties, biocompatibility and tunable longitudinal plasmon wavelengths [13]. Additionally, the electrocatalytic activity of Au NRs is highly dependent on their size and shape, as well as the surrounding mediums. Thus, controlled coating of one metal (shell) over Au NRs (core) is an efficient strategy by which properties of Au NRs can be tuned [14]. Moreover, the shell can be prepared with high monodispersity, yield and precise control of the aspect ratios, resulting in some extraordinary catalytic efficiency [15]. For instances, Au NRs@Pt nanodots core/shell nanostructures have been demonstrated to possess peroxidase or oxidase-like activities and pose promising potentials in various bio/chemical assays [16]. The enhanced activity can be attributed to shell nanoparticles are outstanding catalysts and the cooperative promoting effects. A typical procedure for the growth of Pd shells on Au NRs with remarkably tunable optical responses, making Au NRs@Pt nanodots suitable for sensing applications [17]. But most importantly, the core/shell nanorods could knit a tightly network on the surface of electrode which can not only provide abundant active sites to load analyte [18]. Inspired by the description above, we design AuPd core-shell hybrid nanorods (Au@Pd HNRs) using Au NRs as nucleating centers, and Pd coating was achieved in the growth solution through accurate control of the reduction rate. The Au@Pd HNRs can facilitate the transmission of the electrons between the electrode surface and possess more electrocatalytic sites of the immobilized DA, Tyr and AC, and act as catalysts for electrochemical reactions [19]. For further improve the durability and long-term or recycle catalyze, BG was introduced as excellent carrier effectively prevented the aggregation and migration of Au@Pd HNRs, which has sufficient capability to effectively load Au@Pd HNRs and increased the specific surface of the Au@Pd HNRs/BG hybrid nanocomposites [19]. Particularly, when these nanocomposites were applied to construct electrochemical sensors, they have abilities to accumulate or load DA, Tyr and AC and generate observable electrochemical signals, presenting high selectivity and sensitivity, good precision, acceptable stability and achieved the sensitive determination of DA, Tyr and AC simultaneously with satisfactory results.

2. EXPERIMENTAL

2.1 Reagents

Dopamine, acetaminophen, tyrosine, graphite powder, $NaBH_4$, cetyltrimethylammonium bromide (CTAB), L-ascorbic acid (AA), Boron trioxide powder (B_2O_3, 99%) were from Alfa Aesar without any further treatments. K_2PdCl_4 and gold (III) chloride trihydrate ($HAuCl_4.3H_2O \geq 99.99\%$, wt%) were used for synthesized of Au@Pd HNRs. A 0.1 M phosphate buffer solution (PBS) consisting of KH_2PO_4 and Na_2HPO_4 was employed as the supporting electrolyte. Moreover, High-purity water (18.25 MΩ /cm, Milli-Q) was used in all experiment.

2.2 Instruments and characterizations

UV-vis absorption spectra were measured at Perkin-Elmer Lambda 900 USA, and surface morphologies of BG were characterized by scanning electron microscopy (SEM, Nova Nano SEM 230, FEI, USA). The characteristics of the Au NRs and Au@Pd HNRs were determined using energy-disperse X-ray spectra (EDS). Transmission electron microscope (TEM) and High-resolution transmission electron microscope (HRTEM) image was obtained using Tecnai G2 F20 S-TWIN, 200.0 kV (FEI Company, USA). The elemental compositions and boron -bonding configurations in the BG was carried out with Thermal Scientific K-Alpha XPS spectrometer. All electrochemical experiments including Cyclic voltammetry (CV) and differential pulse voltammetry (DPV) were performed using a CHI 660C electrochemical analyzer (CHI, Shanghai). The electrochemical cell consisted of a three electrode system with a bare glassy carbon electrode (GCE, 3.0 mm in diameter) or modified working electrode as a working electrode, a platinum wire as a counter electrode and Ag/AgCl electrode as a reference electrode.

2.3 Preparation of Au NRs and Au@Pd HNRs

The Au NRs was prepared using modified seed-mediated surfactant-directed method published by K. Park [20] and El-Sayed [21]. Briefly, the seed solution was prepared as by adding a freshly prepared, ice-cold $NaBH_4$ solution (0.6 mL, 0.01 M) into vial with a mixed solution composed of $HAuCl_4.3H_2O$ (5.0 mL, 0.5 mM) and CTAB (5.0 mL, 0.2 M) under vigorous magnetic stirring. For the growth of Au NRs, a growth solution was prepared containing CTAB (5.0 mL, 0.20 M), $HAuCl_4.3H_2O$ (5.0 mL, 1.0 mM) and $AgNO_3$ (0.2 mL, 4.0 mM) at room temperature. Next, 70 μL, 78.8 mM AA was added to the growth solution and mixed thoroughly. Finally, 12 μL of the seed solution and the reaction flask was transferred to the water-bath, which was coated by the cover to avoid the light and the vial left undisturbed 8 h for longitudinal overgrowth.

By controlling the growth environment and the thickness of the Pd shell is tailored through controlled addition of $PdCl_4^{2-}$. In this paper, the Au@Pd HNRs was prepared as follows: two milliliters of Au NRs previously prepared was placed in a beaker equipped with magnetic stirring bars, which containing 75.0 uL of 20.0 mM K_2PdCl_4 and 3.0 mL of water, respectively. The mixtures were stirred thoroughly for at least 10 min in an ice bath (4.0 °C), then a freshly prepared 1.0 mL 0.10 M AA was

added dropwise into the solution under vigorous stirring, then the final solutions were stirred for another 40.0 min, the color of the solution changed from purple to dark gray, suggesting the formation of Pd shell. Finally, the microthermal Au@Pd HNRs were isolated by centrifugation at 3000 rpm repeatedly to remove all precipitated CTAB, the Au@Pd HNRs was washed and centrifuged at 10,000 rpm and redispersed in 5.0 mL of ultra-pure water.

2.4 Preparation of BG and Au@Pd HNRs/BG hybrid nanocomposites

BG was prepared by one-pot hydrothermal synthesis as follows: Firstly, 35.0 mL 0.5 mg/mL GO was sonicated facilitating uniform dispersion, followed by the addition B_2O_3 powder as the source of boron was mixed with GO in a mass ratio of 30:1. Secondly, the resulting mixture was transferred to a Teflon vessel which was held in a stainless-steel autoclave, meanwhile the temperature was increased to 160 ˚C and remained for 3 h. Subsequently, the black floccus products were collected through centrifugation (8000 rpm) and washed three times with alcohol and ultra-pure water, respectively. Finally, the BG was redispersed in 10.0 mL of ultra-pure water.

In a typical synthesis of Au@Pd HNRs/BG hybrid nanocomposites, the above floccus BG (0.5 mL) was dispersed uniformly by using ultrasonic dispersion method for 1.0 h, and 3.5 mL Au@Pd HNRs was add and shaken with a vortex mixer for 2.0 h at room temperature. Due to B doping effect create a large number of defect sites in the basal planes and edges of graphene nanosheets, boron affinity for Au@Pd HNRs embedded in BG nanosheets, thus the well-dispersed Au@Pd HNRs can be successfully decorated on the ultrathin BG nanosheets, forming the Au@Pd HNRs/BG hybrid nanocomposites.

2.5 Fabrication of the electrochemical sensor

For the fabrication of a electrochemical sensor, both BG and Au@Pd HNRs with high specific surface area enough catalytically active sites can immobilize and electro-catalytic more DA. Prior to modification, a GCE was polished with Al_2O_3 to obtain a mirror-like surface and dried under N_2. 7.0 uL of the Au@Pd HNRs/BG hybrid nanocomposites was inserted on the GCE and the solvent has been evaporated naturally at room temperature to obtain Au@Pd HNRs/BG/GCE.

3. RESULTS AND DISCUSSION

3.1 Physicochemical characterization

The growth of Pd nanoparticles on the Au NRs surface could be monitored by UV-vis spectrophotometry (Fig. 1a). The UV–vis spectra of the Au NRs show a longitudinal surface plasma resonance (LSPR) band at 744 nm with a full width at half-maximum of 135 nm and a weak transverse SPR band at 526 nm [22]. After AA was added, Pd ions were gradually reduced and preferentially deposited on the preintroduced Au nanorods, the LSPR band gradually blue-shift to 850.0 nm and albeit severely damped (broadening in peak width and reducing in intensity) due to Au NRs have been

encapsulated by the Pd layer and Pd have no characteristic absorption. On the another hand, the electromagnetic field from the Au core is not completely shielded by the Pd nanoparticles, because of the unique structure of core-shell hybrid nanorods.

The morphology and microstructure of the as-synthesized Au NRs were investigated by TEM in Fig. 1, the homogeneous Au NRs are smooth in appearance and have rounded ends, the average diameter and length is about 13.5 nm and 40.0 nm, respectively (Fig. 1b). HRTEM characterization (Fig. 1c) was conducted to further investigate the crystallographic properties of these Au NRs. A lattice distance of 0.2024 nm corresponds to (200) facets of face-centered cubic (fcc) Au NRs, whereas a lattice distance of 0.2315 nm corresponds to (111) facets.

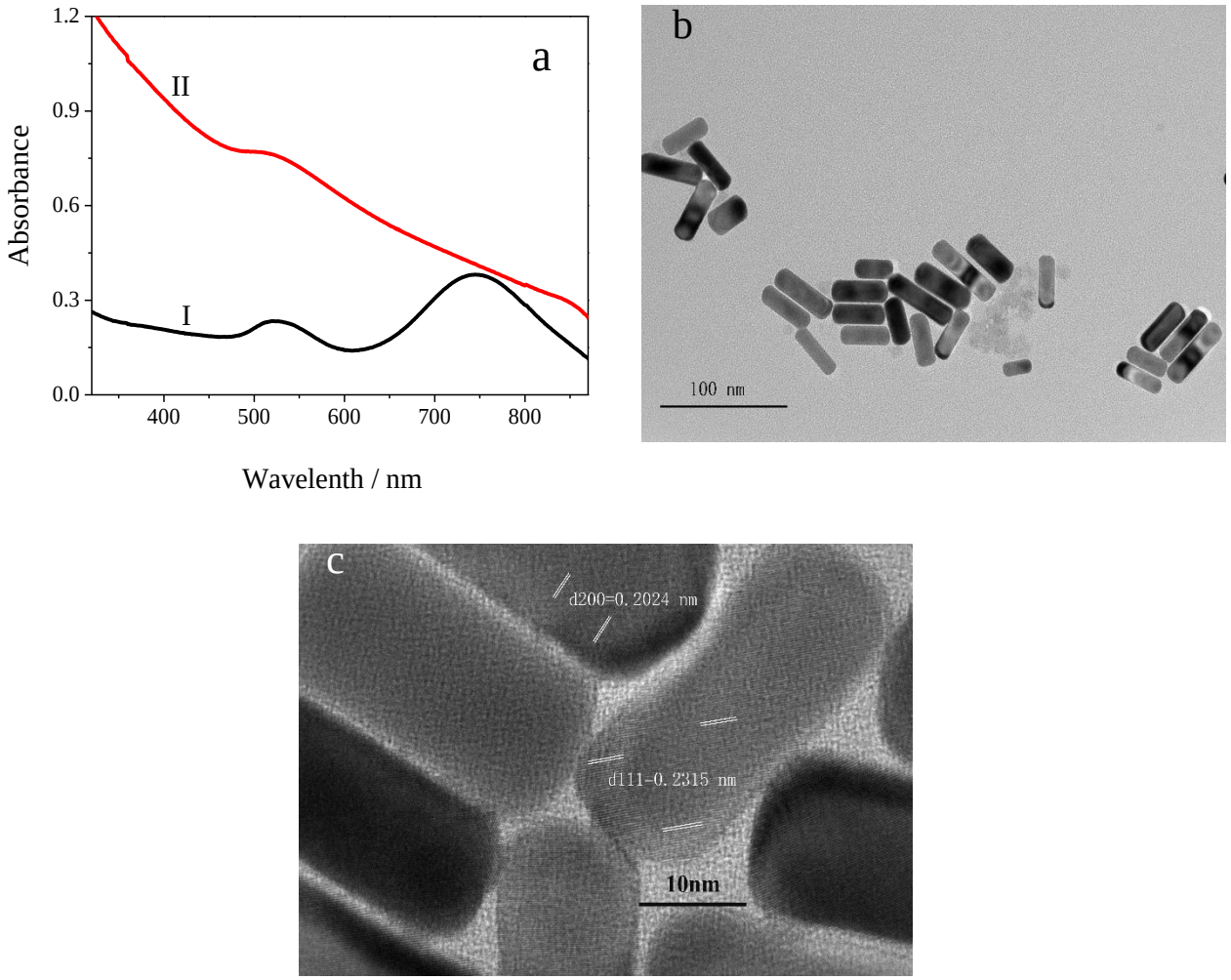

Figure 1. (a) UV-vis spectral sequences of Au NRs (I) and Au@Pd HNRs (II). (b) TEM images corresponding to as-prepared Au NRs. (c) HRTEM image of the Au NRs.

In order to clarify the origin of the optical evolution observed in the overgrowth of Pd, Fig. 2a-d shows the change in morphology as Pd was coated on the Au NRs, the yield of Au@Pd HNRs is nearly 100% with highly disperse, and both of their shape and size are very uniform. However, in comparison with the cylindrical shapes of the Au NRs, all Au@Pd HNRs are rough and displays its own rectangular

with sharp edges in Fig. 2a,b. HRTEM characterization was conducted to further investigate the crystallographic properties of t the as-synthetic Au@Pd HNRs, as shown in Fig. 2c,d, which provide direct evidence of the crystal structure of the Pd shell with the diameter is about 2–5 nm. In Fig. 2c, Au@Pd HNRs showed a fairly The peculiar structure uniform morphology with Pd shell-shaped structure at the periphery. In addition, tens of small Pd nanoparticles are formed over Au NRs, resulting two Au@Pd HNRs are connected together. Interestingly, the Pd shell grows epitaxially around the Au NR and is thus a single-crystal structure, a lattice distance of 0.225 nm corresponds to (111) facets of fcc Pd in Fig. 2d, which shows the contrast in the core and outer shell, further confirms that the Au@Pd HNRs adopt a core/shell structure. not only provided multiple electron pathways, but also possessed enlarged electroactive surface area for the immobilization and electrocatalysis of DA, Tyr and AC.

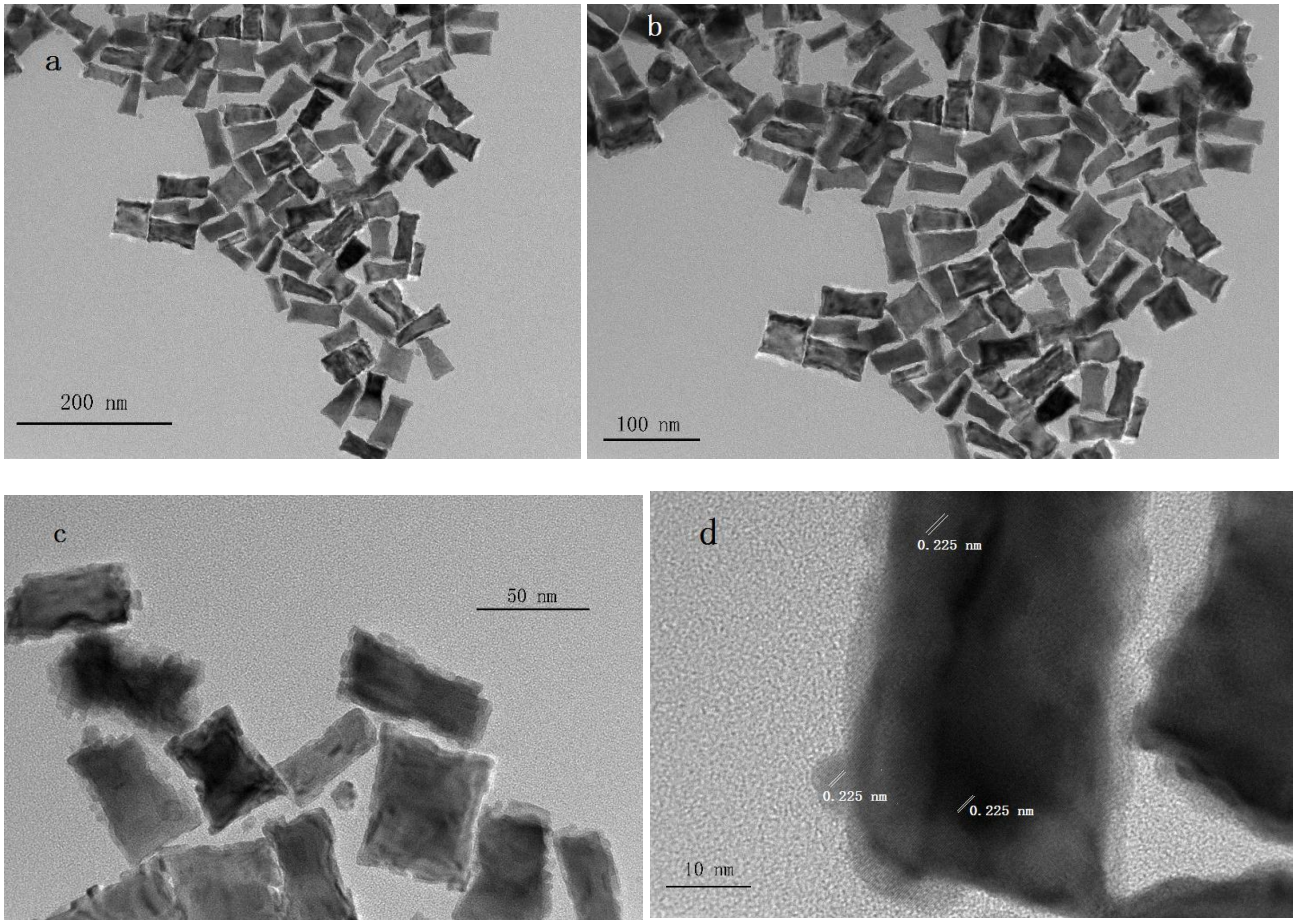

Figure 2. Typical TEM image of Au@Pd HNRs at different magnifications (a,b,c). HRTEM image displaying the lattice fringes of the Au@Pd HNRs (d).

The representative SEM image of BG displayed a two-dimensional sheet-like structure with porous, ultrathin features and crinkles (Fig. 3a). Moreover, the detailed information on the near-surface elemental compositions of BG was further revealed by XPS in Fig. 3b-e. As shown in the full scan XPS spectrum (Fig. 3b), the BG nanosheets have a binding energy peak (B1s) at 192.17 eV, and the predominant C1 s peak located at 284.17 eV, O1 s peak at ca. 532.17 eV, the higher binding energy of

BG (the binding energy of pure boron is 187.00 eV) indicates that the B atoms are bonded to carbon atoms in the sp^2 carbon network [23]. Additionally, it is revealed that the atomic percentage of boron in BG is around 2.53 at%. In Fig. 3c, four obvious spectral peaks shown in the core level spectra of C1s for the BG at 284.62 eV (represent the sp^2-hybridized carbon peak), 285.10 eV (the presence of C−C, C−O and C–B), 286.22 eV (C–O moieties such as epoxy and hydroxyl groups on the basal planes) and 289.35 eV (C–O–B and O–C=O or –COOH), respectively.

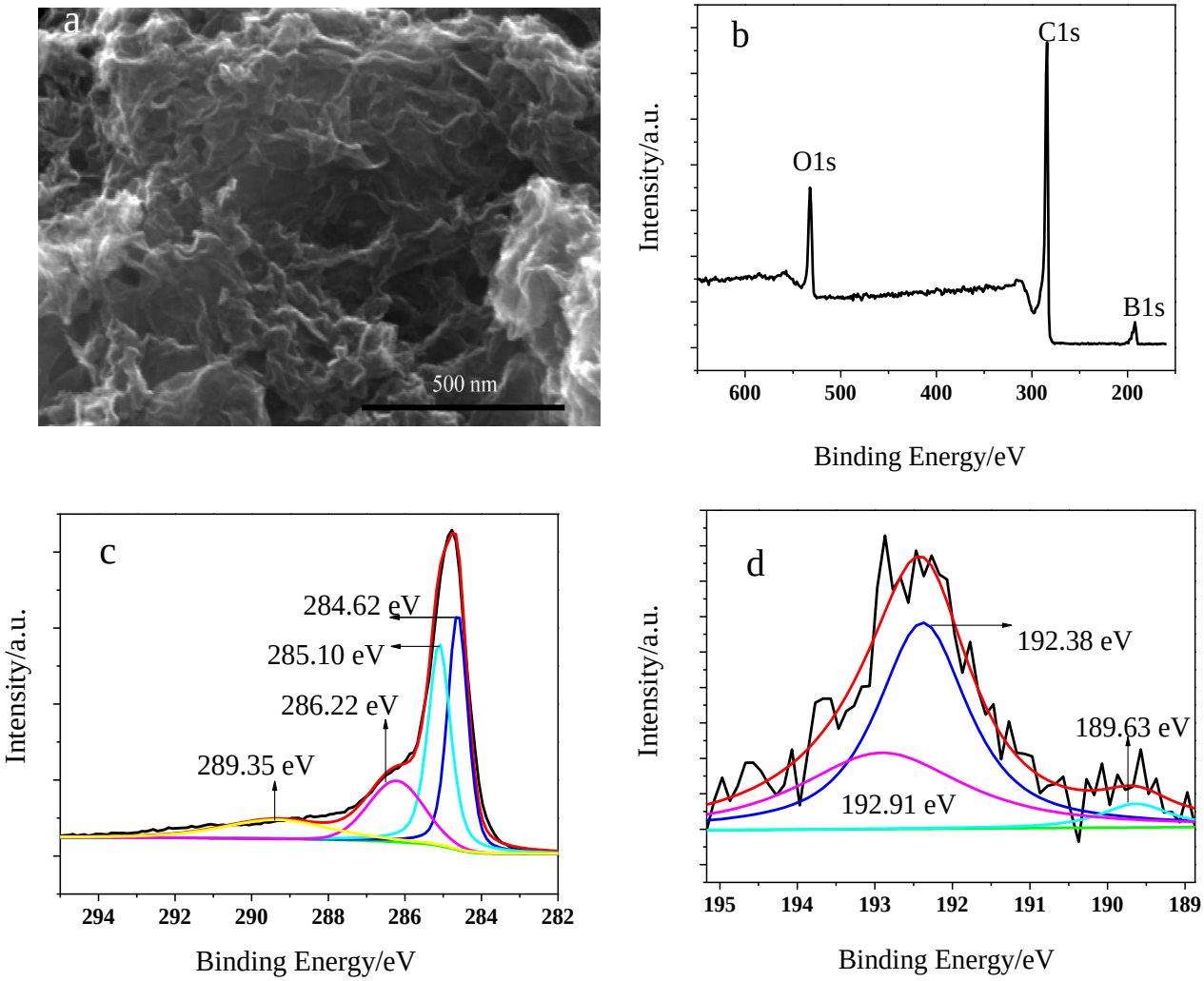

Figure 3. SEM images of B-doped graphene at different magnifications (a). (b) XPS surveyspectrum of BG. Deconvoluted C1s (c), B1s (d) and O1s (e) of XPS spectrum of BG.

Fig. 3d exhibits the normalized high resolution spectra of the B1s core level for the BG, it can be deconvoluted into three peaks centered at 189.63, 192.38 and 192.91 eV namely B−C, BCO_2 or BC_2 and B−O bonds, respectively. The presence of BCO_2 and BC_2 bonds suggest that the B atom doped at the defect sites of graphene [24], boron−oxygen-carbon compounds are easily formed when B adopts a low coordinated substitutionalsite along graphene edges and, more limitedly, to boron oxide [25]. For the

O1s peak, three subpeaks can be found at 533.55, 532.39 and 531.16 eV, representing HO−C=O, C=O and C−OH or C–O–C bonding (Fig. 3e). The O/C atomic ratio for the BG is ca. 16.41%, suggesting that BG with excellent hydrophilicity will beneficial to form hydrogen bonding with phenolic hydroxyl group of DA, Tyr and AC, which not only highly offered the capability of targeting for DA, Tyr and AC but also enhance effectively the sensitivity of an electrochemical sensor.

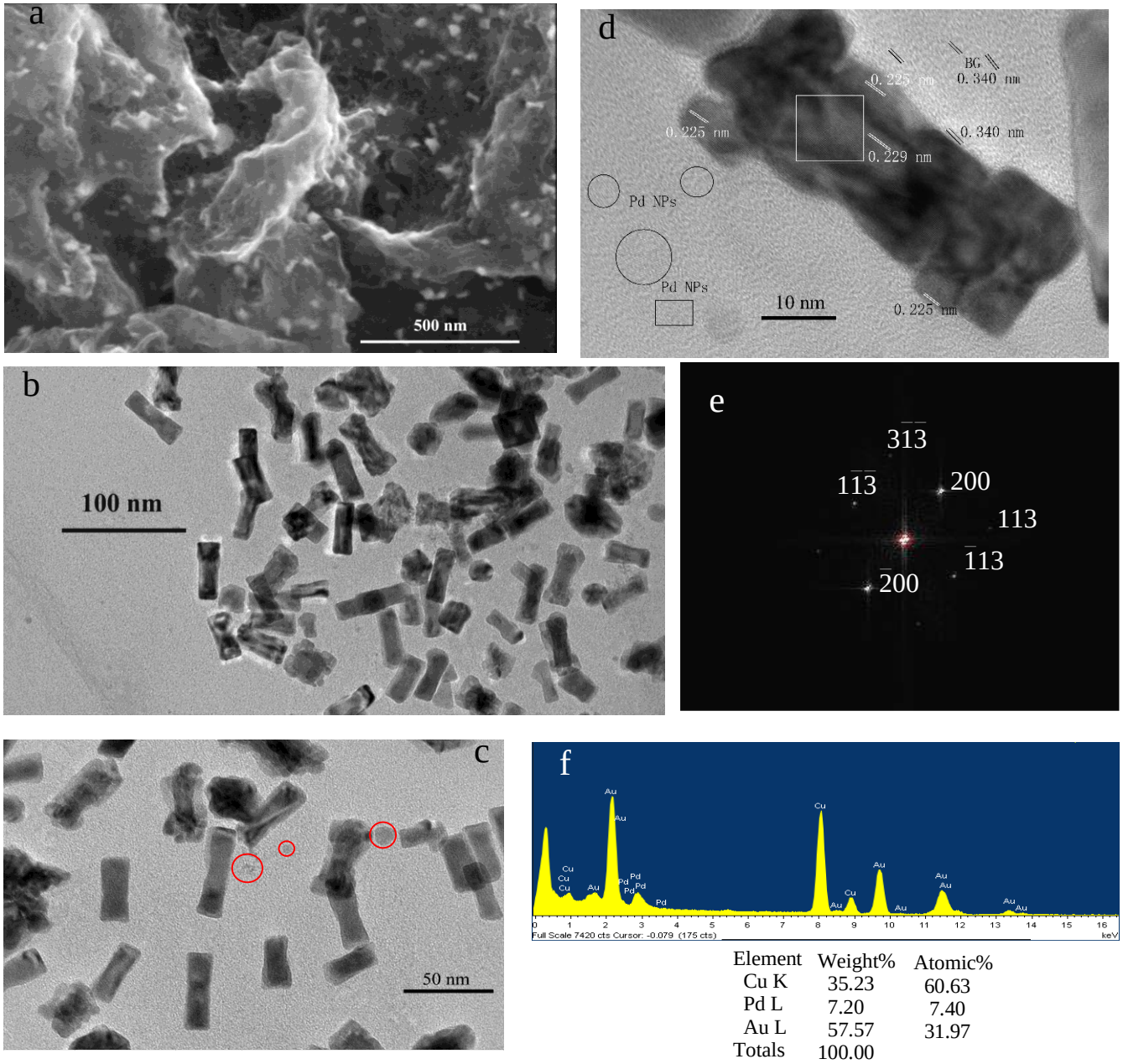

Element	Weight%	Atomic%
Cu K	35.23	60.63
Pd L	7.20	7.40
Au L	57.57	31.97
Totals	100.00	

Figure 4. SEM image of Au@Pd HNRs/BG (a). TEM (b) and HRTEM (c) images of the Au@Pd HNRs/BG nanocomposites at different magnifications. (d) HRTEM image displaying the lattice fringes of the Au@Pd HNRs/BG nanocomposites. (e) Diffraction patterns of Au@Pd HNRs for different directions. (f) EDX analysis for Au@Pd HNRs (Cu from the copper grid).

Fig. 4 shows the SEM and TEM image of the Au@Pt HNRs/BG hybrid nanocomposites. The

wrinkled nature and uniform decoration of Au@Pt HNRs embedded in BG (Fig. 4a) has been observed by SEM. As the TEM images show in Fig. 4b, the Au@Pt HNRs were encapsulated in the BG sheets with well dispersion and kept uniform in size and shape, meanwhile the paper-like ultrathin, transparent and wrinkled BG nanosheets were propped open further by Au@Pt HNRs. From HRTEM image (Fig. 4c), the morphology and microstructure of the as-synthesized Au@Pt HNRs/BG hybrid nanocomposites was observed clearly, the Au@Pd HNRs with less degree of agglomeration were anchored on BG folded surface, representing the elongated black spots. As observed, a few Pd nanoparticles on BG are smaller than Au@Pd HNRs, it can be assumed again the formation mechanism of the three-dimensional Au@ HNRs is that tens of small Pd nanoparticles deposit on Au NRs surface. In order to observe more clearly, viewing from the enlarged HRTEM image in Fig. 4d, i the lattice spacing values of Au core and shell are Pd 0.229 and 0.225 nm, corresponding to the mean value of the (111) planes of face-centered cubic (fcc) Au and Pd [26], around which is the (002) crystal faces of BG with lattice spacing of 0.340 nm. Moreover, the interface between graphene and Au@Pd HNRs can be clearly observed. To further confirmed the growth direction of Pd nanoparticles on Au NRs surface, the corresponding fast Fourier transform (FFT) pattern at the location are marked by "white frame" in Fig. 4d was acquired (Fig. 4e), the spots are indexed corresponding to the (313), (200), (113), (113) (200) and (113), reflections of Au with zone axes (ZA) of [031], which confirmed that the growth direction of Pd was along [100] direction on both sides of the Au rod [27].

Moreover, EDS results (Fig. 4f) clearly indicate that the rectangular-shaped nanostructure was composed of Au and Pd (Cu stem from copper grid), and the Pd does indeed continue to grow more at the ends of the Au rods. In conclusion, it is obvious that the Au@Pd HNRs with a certain aspect ratio are homo-dispersed on the surface of BG are propped open further by Au@Pd HNRs, which can increase the surface-to-volume ratio of BG and provide a broader platform for efficiently capturing more DA, Tyr and AC.

3.2 Electrochemical behavior of DA, Tyr and AC in a ternary mixture

It is well known that the electrochemical detection of DA, Tyr and AC on ordinary electrodes is hard due to their oxidation potentials are so close that resulting in an overlapped voltammetric response and hard to distinguish their signals peaks [28]. Hence, Au@Pt HNRs/BG hybrid nanocomposites was used as a highly sensitive accumulation platform and signal amplifier in this paper, which achieve the increased potential difference make them possible to discriminate. The CV and DPV recorded for DA (0.012 mM), AC (0.030 mM) and Tyr (0.125 mM) from Au@Pd HNRs/BG/GCE are shown in Fig. 5. From Fig. 5A, voltammogram a shows two irreversible redox peaks for DA, however, the reduction peaks for AC and Tyr are indistinguishable. The oxidation peak of DA, AC and Tyr appeared at about 0.38 V, 0.60 V and 0.82 V, respectively. The reduction peak of DA appeared at the potential of 0.20 V, which consistent with former literatures [29,30]. DPV of DA, AC and Tyr is shown in Fig. 5B, three separated peaks with well-defined shapes and large oxidation peak currents were observed at Au@Pd HNRs/BG/GCE. The oxidation peaks of DA, AC and Tyr appeared at 0.30, 0.58 and 0.80 V, the separation of the oxidation peak potentials for DA-AC, DA-Tyr and AC-Tyr are 280, 500 and 220 mV,

respectively. It can be clearly observed that simultaneous determination of the three species can be possible, which was free from mutual interferences. These synergistic amplification effect can be effectually enhanced in boron affinity for Au@Pd HNRs embedded into BG nanosheets with highly dispersed –COOH groups and their cooperative promoting effects.

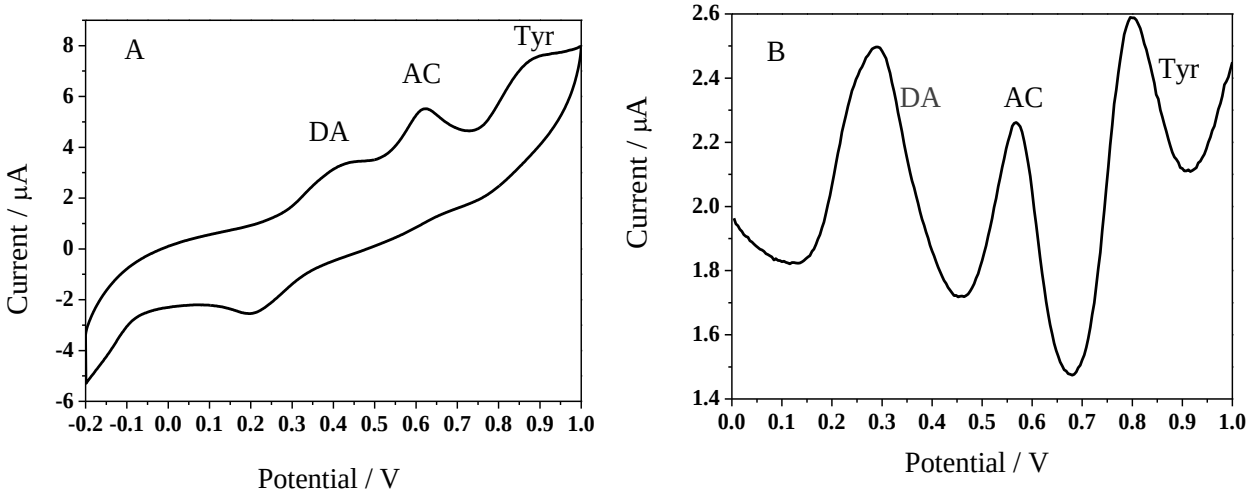

Figure 5. CV (A) and DPV (B) of Au@Pd HNRs/BG/GCE in the mixture containing 0.012 mM DA, 0.030 mM AC and 0.125 mM Tyr in 0.1 M 20 mL PBS (pH 7.4) at the scan rate of 50 mV/s.

3.3. Effect of pH on the oxidation of DA, AC and Tyr

Since DA, AC and Tyr contain phenolic group on their structure, the protons can took part in the electrode reaction process, therefore the most desirable pH is very important for detection of these species. Fig. 6A-C illustrates the effect of solution pH on the peak current responses of DA, AC and Tyr, respectively. The results indicate that proton influenced peaks current and potential, and the anodic peak potential shifted negatively with the increased pH value due to proton takes part in the electrode reaction processes of the analytes. Moreover, the corresponding anodic peak potentials for DA, AC and Tyr vary linearly with pH and the linear regression equations are presented in below:

E_{pa}=0.595-0.050 pH R^2=0.986

E_{pa}=0.973-0.056 pH R^2=0.994

E_{pa}=1.493-0.065 pH R^2=0.986

In addition, the cathodic peak potential for AC and the pH values existed linear relationships, linear regression equations between E_{pc} and pH value was E_{pc}=0.971-0.057 pH (R^2=0.995). All the slopes were close to the Nernestian value of 59 mV pH^{-1}, which suggest that the electro-oxidation reactions involved two electrons and two protons mechanism [31,32]. Fig. 6D showed that the oxidation peak currents for DA, AC and Tyr increased gradually with an increase in pH, and maximum peak current occur at pH 7.4. Therefore, pH 7.4 was chosen as the most desirable pH for subsequent experiments.

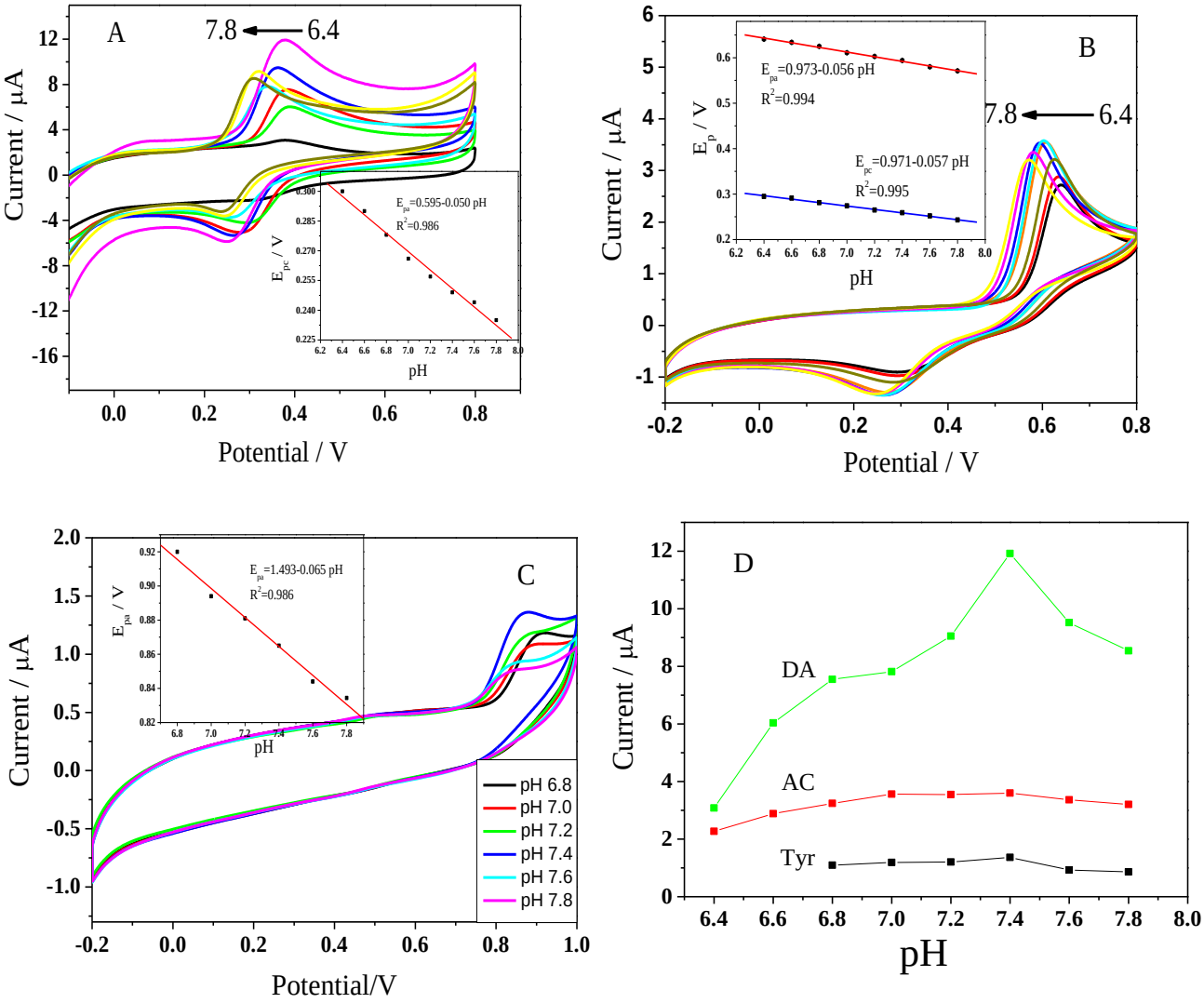

Figure 6. CVs obtained at the Au@Pd HNRs/BG/GCE in PBS with different pH values (6.4, 6.6, 6.8, 7.0, 7.2, 7.4, 7.6 and 7.8) containing 0.075 mM DA (A), 0.300 mM AC (B) and with different pH values (6.8, 7.0, 7.2, 7.4, 7.6 and 7.8) containing 0.300 mM Tyr (C) at scan rate of 50 mV/s. Inset: the plots of peak potential (E_p) of these compounds versus pH values. Influence of pH values on the current response of three species at the Au@Pd HNRs/BG/GCE (D).

3.4. Effect of scan rate

In order to investigate the mechanisms for the electrochemical oxidation of DA, AC and Tyr at Au@Pd HNRs/BG/GCE, the relationship between the peak currents and scan rate (30~190 mV s^{-1}) of potential sweep were recorded in Fig. 7A-C. It is noticeable that by increasing scan rate, both the peak potential and peak current are affected, the redox peak current of DA and AC as well as the anodic peak current of Tyr increased gently, and the anodic peak potentials (E_{pa}) shifted to more positive potentials, while the cathodic peak potentials (E_{pc}) shifted negatively. The oxidation peak currents of DA, AC and Tyr vary linearly with scan rates, which revealed the oxidation process of DA, AC and Tyr on the surface of Au@Pd HNRs/BG/GCE were adsorption-control process.

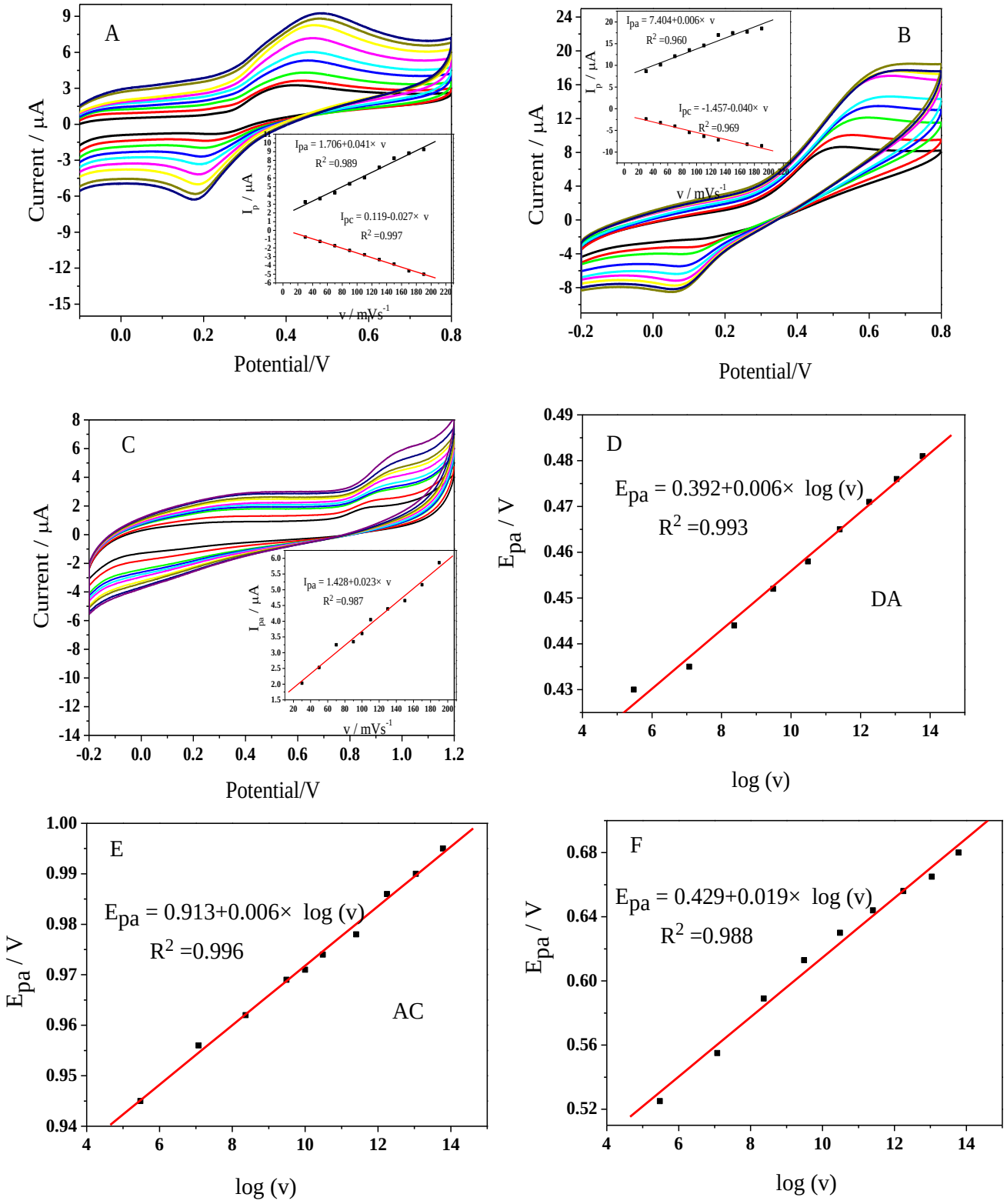

Figure 7. CVs obtained at the Au@Pd HNRs/BG/GCE in 0.1 M 20 mL PBS (pH 7.4) at different scan rates (30~190 mV s^{-1}) containing 0.160 mM DA (A), 0.045 mM AC (B) and 0.200 mM Tyr (C). The relationship between the oxidation peak potential (E_{pa}) and log (v) of DA (D), AC (E) and Tyr (F).

Moreover, the E_{pa} of DA, AC and Tyr were proportional to the logv, based on Laviron theory the charge transfer coefficient (α) can be determined by measuring the plot E_p versus log (v) [33]. According to the equations of E_{pa}= K+2.303(RT/α_anF)log(v) and the slopes of E_{pa} vs. log(v) for DA, AC and Tyr as shown in Fig. 7D-F, by considering two electrons transferred for DA, AC and Tyr, and α of 4.93 for DA and AC, 1.56 for Tyr were obtained, respectively.

3.5. Selective determination of DA, AC and Tyr

To verify the feasibility of the synchronous determination of DA, AC and Tyr by the Au@Pd HNRs/BG/GCE, the DPVs carried out in the mixtures by changing the concentration of one species and the others was kept constant. Typical DPVs of different concentration of DA in the presence of 300.00 μM Tyr and 100.00 μM AC on the Au@Pd HNRs/BG/GCE was presented in Fig. 8A, the oxidation peak current of DA linearly increases with the increase in DA concentration in the range 50.00−275.00 μM with a linear function I_p(μA)=0.005c(μM) +1.145, R^2=0.993 (Fig. 8B), while the oxidation peak currents for Tyr and AC keep nearly unchanged. It's worth noting that Tyr and AC have no interfering effect on the detection of DA. As displayed in AC in the presence of 6.25 μM DA and 150.00 μM Tyr was shown in Fig. 8C, with the increase in AC concentration from130.00 to 1010.00 μM, the oxidation peak current of AC exhibits a linear increase, while the oxidation peak currents for DA are almost constant. The linear regression equations is expressed as: I_p(μA)=0.004c(μM)+3.213, R^2=0.995 (Fig. 8D). Similarly, as shown in Fig. 8E, the increase of Tyr concentration led to the increases of their peak currents, but had no significant influence on the peak of 6.25 μM DA and 150.00 μM AC. The anodic peak current exhibited a linear response to the increasing concentration of Tyr in the range of 30.00−360.00 μM, and the linear equation can be elucidated as: I_p(μA)= 0.004 c(μM)+0.668, R^2=0.997 (Fig. 8F). Interesting, in Fig. 8C by increasing the concentration of Tyr, the oxidation potentials for Tyr is to some extent shifting, indicating that protons take part in their electrode reaction process [30].

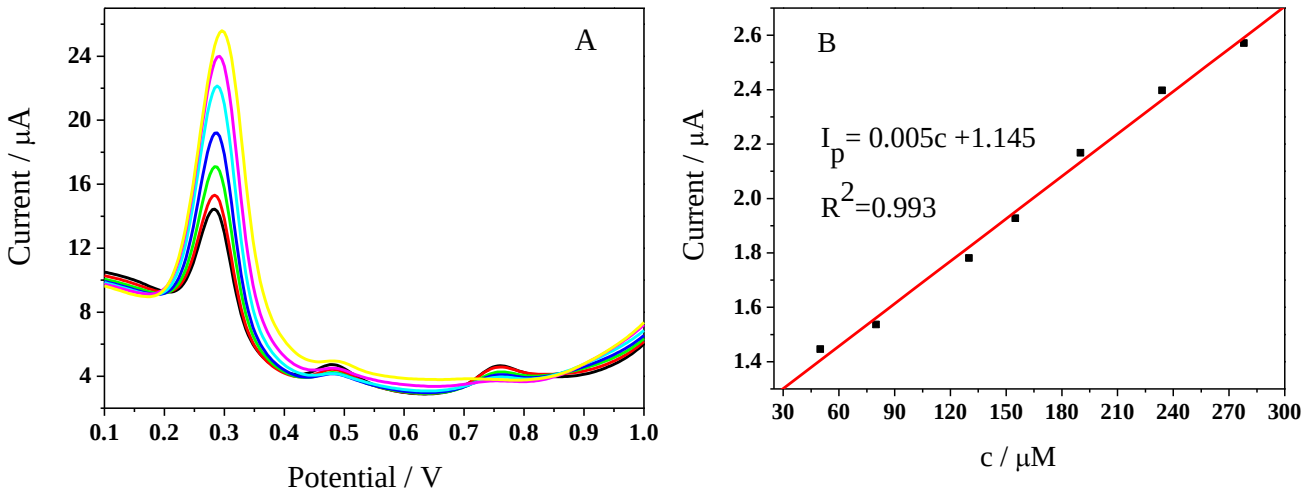

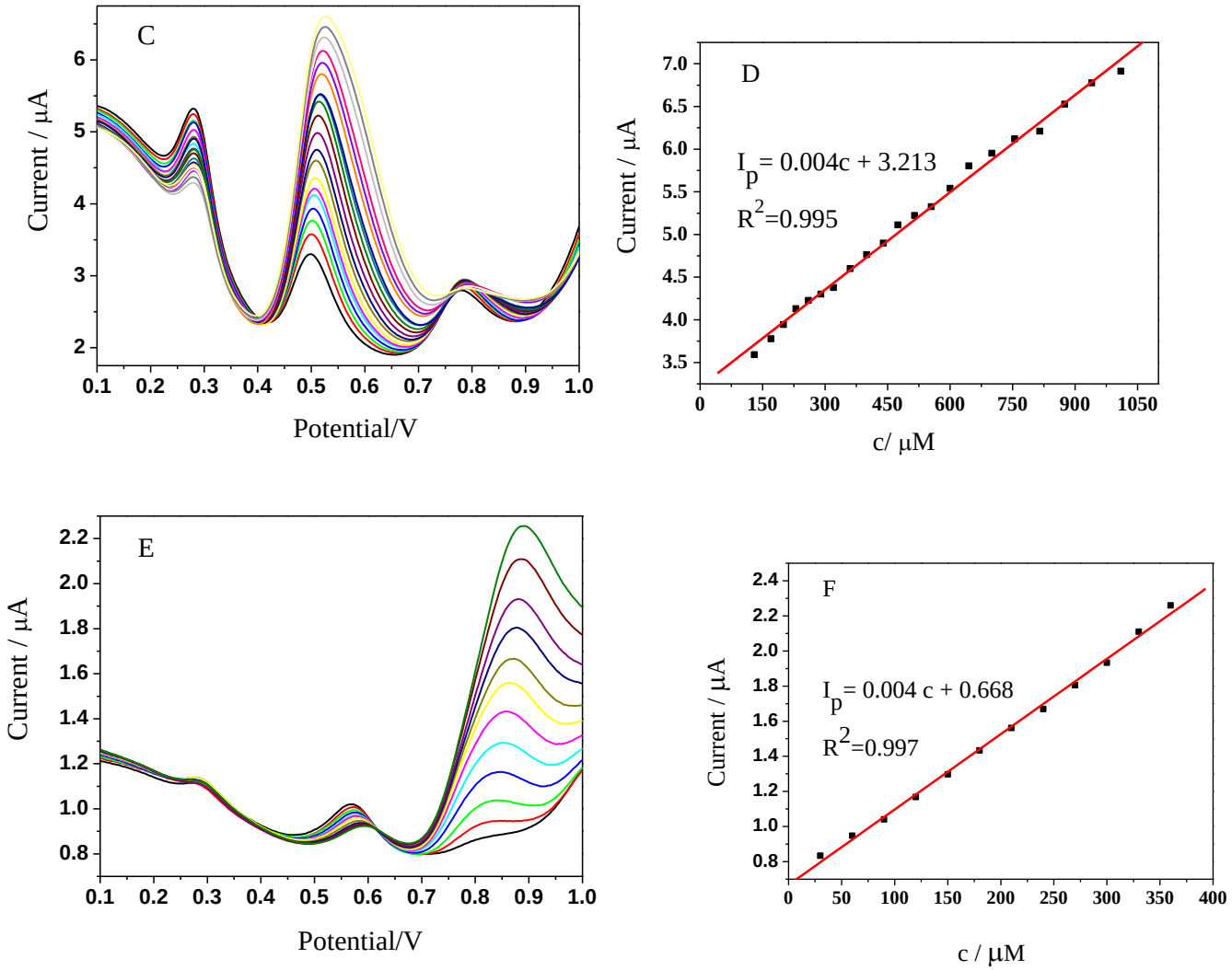

Figure 8. DPVs at Au@Pd HNRs/BG/GCE in 0.1 M 20 mL PBS (pH 7.4) (A) containing 300.00 μM Tyr, 100.00 μM AC and different concentrations of DA (from 1 to 8): 50.00 μM, 80.00 μM, 130.00 μM, 155.00 μM, 180.00 μM, 235.00 μM and 275.00 μM. (B) containing 6.25 μM DA, 150.00 μM Tyr and different concentrations of AC (from 1 to 8): 130.00 μM, 170.00 μM, 200.00 μM, 230.00 μM, 260.00 μM, 290.00 μM, 320.00 μM, 360.00 μM, 400.00 μM, 440.00 μM, 475.00 μM, 515.00 μM, 555.00 μM, 600.00 μM, 645.00 μM, 700.00 μM, 755.00 μM, 815.00 μM, 875 .00 μM, 940.00 μM and 1010.00 μM. (C) containing 6.25 μM DA, 150.00 μM AC and different concentrations of Tyr (from 1 to 9): 30.00 μM, 60.00 μM, 90.00 μM, 120.00 μM, 150.00 μM, 180.00 μM, 210.00 μM, 240.00 μM, 270.00 μM, 300.00 μM, 330.00 μM and 360.00 μM.

The detection limits (S/N=3) for determination of DA, AC and Tyr were found to be 4.58, 6.35 and 3.71 μM, respectively. Table 1 gives the comparison of the different modified electrodes used in the determination of DA, AC and Try with other previous literatures [34-36], the application of Au@Pd HNRs/BG hybrid electrocatalysts for simultaneous determination of DA, AC and Tyr has rarely been explored. Based on this comparison the presented Au@Pd HNRs/BG/GCE owns its unique properties.

Table 1. Response properties of determination of DA, AC and Tyr with different modified electrodes.

Electrode material	Detection limit (μM)			Linear range (μM)			Refs.
	DA	AC	Tyr	DA	AC	Tyr	
GC/p-APT/RGO	–	–	5.97	–	–	50–600	[34]
Pyrolytic carbon (PyC) film	2.3	1.4	5.97	18–270	15–225	–	[35]
Fe_2O_3	0.12	0.1		60–600	10–800	–	[36]
Au@Pd HNRs/BG	4.58	6.35	3.71	50.00–275.00	130.00–1010.00	30.00–360.00	This work

3.6. Stability, repeatability, and reproducibility of Au@Pd HNRs/BG/GCE

The reproducibility of the Au@Pd HNRs/BG/GCE was studied by DPV, and relative standard deviations (RSD) of 2.17%, 1.91% and 2.56% for five equally Au@Pd HNRs/BG/GCE determinations of 0.012 mM DA, 0.030 mM AC and 0.125 mM Tyr in the mixture were obtained, respectively. The repeatability of the proposed sensor was examined by a series of 20 successive DPV measurements in the ternary mixture, the RSD in peak currents were found to be 2.9%, 3.1% and 3.5% for 0.012 mM DA, 0.030 mM AC and 0.125 mM Tyr, respectively, indicating that the Au@Pd HNRs/BG/GCE is not subject to surface fouling. The long-term stability of the Au@Pd HNRs/BG/GCE was tested by storing them for 10 days at room temperature and DPVs were recorded, the comparisons revealed the peak currents were less than 5.0% decrease in the oxidation signals for DA, AC and Tyr, which shows enhanced good stability and durability profiting from the stress effect caused by lattice mismatch of Au and Pd [14]. The Au@Pd HNRs/BG/GCE show highly reproducibility and stability for simultaneous determination DA, AC and Tyr can be concluded that the preparation of BG via hydrothermal approach could introduce highly dispersed COOH groups and defect sites, which not only improve the interfacial properties of Au@Pd HNRs and effectually improve the catalytic effect the three analytes.

3.7. Real sample analysis

To assess the analytical applicability and accuracy of the proposed Au@Pd HNRs/BG/GCE, determination of DA, AC and Tyr was done in the urine sample by the standard addition method. Prior to measurement process, the urine sample was diluted 100 times with 0.10 M pH 7.4 PBS to fit the calibration curve and also and stored in refrigerator until analytical measurements. 10 μL of the diluted urine sample was added into 10 mL 0.10 M pH 7.4 PBS blank, the standard DA, AC and Tyr solution were added in the diluted urine sample by DPV method. The standard-solution additions yielded a good average recovery (94.7−104.6%) for DA, AC and Tyr (Table 2), which clearly verifies the practical applicability and reliability of the present modified electrode.

Table 2. Determination results of DA, AC and Tyr in the urine sample (n=3) with Au@Pd HNRs/BG/ GCE.

Sample	Analyte	Added (μM)	Found (μM)	Recovery (%)
Urine	DA	5.00	5.23	104.6
	AC	8.00	8.05	100.6
	Tyr	10.00	9.47	94.7

4. CONCLUSIONS

A novel Au@Pd HNRs/BG hybrid nanocomposites was synthesized for the simultaneous determination of DA, AC and Tyr. Firstly, a series of Au@Pd HNRs was prepared by controlled overgrowth of Pd shell on pre-introduced Au NRs serving as seeds. Secondly, a one-pot hydrothermal approach for preparation of BG with highly dispersed COOH groups and abundant defect sites, thus the Au@Pd HNRs were facilely encapsulated in BG to form Au@Pd HNRs/BG hybrid nanocatalysts with excellent dispersibility. Moreover, the −COOH units can form hydrogen bonding with the phenolic hydroxyl groups of DA, AC and Tyr, providing a large effective surface area to increase the loading amount and improve the excellent electro-catalytic effect the three analytes. Therefore, the wide potential differences for DA-AC, DA-Tyr and AC-Tyr are about 280, 500 and 220 mV, respectively. The calibration curves for DA, AC and Tyr were obtained in the range of 50.00−275.00 μM, 130.00−1010.00 μM, and 30.00−360.00 μM, respectively. The detection limits (S/N=3) for determination of DA, AC and Tyr were found to be 4.58, 6.35 and 3.71 μM, respectively. Eventually the electrochemical sensor was used successfully for the simultaneous determination of DA, AC and Tyr in the urine sample.

ACKNOWLEDGMENTS
The authors gratefully acknowledge the financial support from the Yunnan education department of Scientific Research Foundation (2018JS478), Yunnan Local Colleges Applied Basic Research Projects (2018FH001-114), the National Natural Science Foundation of China (21665008), the Youth project of Yunnan Province (No 2014FD054), the training program of Young academic and technical talent reserve in Yunnan province (2018HB005), and Innovative Research Team (in Science and Technology) in University of Yunnan Province. This work was supported by the Yunnan Applied Basic Research Project (No. 2018FH001-049) and Yunnan Province Department of Education Fund (No. 2019J1183).

References

1. W.H. Cai, J.W. Lai, T. Lai, H.T. Xie and J.S. Ye, *Sens. Actuators*, B, 224 (2016) 225.
2. K. Tyszczuk-Rotko, I. Jaworska, K. and Jędruchniewicz, *Microchem. J*., 146 (2019) 664.
3. F. Tadayon, S. Vahed and H. Bagheri, *Mater. Sci. Eng*. C, 68 (2016) 805.
4. A.K. Bhakta, R.J. Mascarenhas, O.J. D'Souza, A.K. Satpati, S. Detriche, Z. Mekhalif and J. Dalhalle, *Mater. Sci. Eng*. C, 57 (1) (2015) 328.
5. M.D. Tezerjani, A. Benvidi, A.D. Firouzabadi, M. Mazloum-Ardakani and A. Akbari, *Measurement*, 101(2017) 183.
6. A. Cernat, M. Tertiş, R. Săndulescu, F. Bedioui, A. Cristea and C. Cristea, *Anal. Chim. Acta*, 886

(2015) 16.
7. M.R. Majidi, M.H. Pournaghi-Azar and R. F.B. Baj, *J. Mol. Liq.,* 220 (2016) 778.
8. H. Karimi-Maleh, M.R. Ganjali, P. Norouzi and A. Bananezhad, *Mater. Sci. Eng. C,* 73 (2017) 472.
9. H.R. Zare, B. Moradiyan, Z. Shekari and A. Benvidi, *Measurement*, 90 (2016) 510.
10. N. Baig, M. Sajid and T. A. Saleh, TrAC, *Trends Anal. Chem*., 111(2019) 47.
11. B.D. Liu, X.Q. Ouyang,Y.P. Ding, L.Q. Luo, D. Xu and Y.Q. Ning, *Talanta*,146 (2016)114.
12. M. Taei and G. Ramazani, *Colloids Surf.,* B, 123 (2014) 23.
13. T. Lin, Z. Li, Z. Song, H. Chen, L.Q. Guo, F. Fu and Z. Wu, *Talanta*, 148 (2016) 62.
14. Y.Y. Deng, H.R. Xue, S.L. Lu, Y.J. Song, X.Q. Cao, L. Wang, H.J. Wang, Y.L. Zhao and H.W. Gu, *ACS Appl. Energy Mater.*, 1 (9) (2018) 4891.
15. C.H. Fang, T. Bi, Q. Ding, Z.Q. Cui, N. Yu, X.X. Xu and B.Y. Geng, *ACS Appl. Mater. Interfaces*, 11(22) (2019) 20117.
16. J.B. Liu, X. N. Hu, S. Hou, T. Wen, W.Q. Liu, X. Zhu, J.-J. Yin and X.C. Wu, *Sens. Actuators*, B, 166-167 (2012) 708.
17. S. Rodal-Cedeira, V. Montes-García, L. Polavarapu, D.M. Solís, H. Heidari, A.L. Porta, M. Angiola, A. Martucci, J. M. Taboada, F. Obelleiro, S. Bals, J. Pérez-Juste and I. Pastoriza-Santos, *Chem. Mater.*, 28 (2016) 9169.
18. X. Lu, L. Tao, Y.S. Li, H.M. Huang and F.M. Gao, *Sens. Actuators*, B, 284 (2019) 103.
19. C. Wang, L.Y. Hu, K. Zhao, A.P. Deng and J.G. Li, *Electrochim. Acta*, 278 (2018) 352.
20. K. Park, L.F. Drummy, R.C. Wadams, H. Koerner, D. Nepal, L. Fabris and R.A. Vaia, *Chem. Mater.*, 25 (2013) 555.
21. B. Nikoobakht and M.A. El-Sayed, *Chem. Mater*., 15 (2003) 1957.
22. Z.H. Xia, P.F. Li, Y.S. Wang, T. Song, Q. Zhang and B.Q. Sun, *ACS Appl. Mater. Interfaces*, 7 (2015) 24136.
23. Y.Z. Zhang, R.X. Sun, B.M. Luo and L.J. Wang, *Electrochim. Acta*, 156 (2015) 228.
24. Y.R. Sun, C.Y. Du, M.C. An, L. Du, Q. Tan, C.T. Liu, Y.Z.Gao and G.P. Yin, *J. Power Sources*, 300 (2015) 245.
25. M. Cattelan, S. Agnoli, M. Favaro, D. Garoli, F. Romanato, M. Meneghetti, A. Barinov, P. Dudin and G. Granozzi, *Chem. Mater*., 25 (2013) 1490.
26. X.L. Chen, H.B. Pan, H.F. Liu and M. Du, *Electrochim. Acta*, 56 (2010) 636.
27. X. Ma, M.-C. Wang, J.Y. Feng and X.J. Zhao, *J. Alloys Compd*, 637 (2015) 36.
28. B. Habibi, M. Jahanbakhshi and M. H. Pournaghi-Azar, *Electrochim. Acta*, 56 (2011) 2888.
29. F. Tadayon , S. Vahed and H. Bagheri, *Mater. Sci. Eng.* C, 68 (2016) 805.
30. T. Madrakian, E. Haghshenas and A. Afkhami, *Sens. Actuators*, B, 193 (2014) 451.
31. X.L. Chen, W. Liu, L.L. Tang, J. Wang, H.B. Pan and M. Du, *Mater. Sci. Eng*. C, 34 (2014) 304.
32. N.F. Atta, Y.M. Ahmed and A. Galal, *J. Electroanal. Chem*., 828 (2018)11.
33. A. Babaei, A. Yousefi, M. Afrasiabi and M. Shabanian, *J. Electroanal. Chem*., 740 (2015) 28.
34. H.-B. Noh, S.B. Revin and Y.-B. Shim, *Electrochim. Acta* 139 (2014) 315.
35. G.P. Keeley, N. McEvoy, H. Nolan, S. Kumar, E. Rezvani, M. Holzinger, S. Cosnier and G.S. Duesberg, *Anal. Method*., 4 (2012) 2048.
36. P.N. Manikandan and V. Dharuman, *Electroanalysis*, 29 (2017) 1.